Determining the Lithium Local Environments in the Lithium Manganates $LiZn_{0.5}Mn_{1.5}O_4$ and Li_2MnO_3 by Analysis of the ^6Li MAS NMR Spinning Sideband Manifolds

Young Joo Lee and Clare P. Grey*

Department of Chemistry, State University of New York at Stony Brook, Stony Brook, New York 11794-3400

Received: August 20, 2001; In Final Form: January 10, 2002

Li_2MnO_3 and the spinel $LiZn_{0.5}Mn_{1.5}O_4$ each contain a subset of lithium ions in very similar octahedral environments, in terms of the Li−O−Mn connectivities (i.e., numbers of nearby manganese ions and Li−O−Mn bond angles). We show, however, that the different geometric arrangements of the Mn ions about the lithium ions lead to very different spinning sideband manifold patterns, providing a simple method for distinguishing between the two different local environments. The dipolar coupling tensors which describe the coupling between the electron and nuclear magnetic moments are determined for the 2b site in Li_2MnO_3 and the octahedral site in $LiZn_{0.5}Mn_{1.5}O_4$, on the basis of the crystallographic structures, and the spinning sideband patterns are calculated. Two types of axial symmetry, i.e., oblate and prolate symmetry, for the sites in Li_2MnO_3 and $LiZn_{0.5}Mn_{1.5}O_4$, respectively, are obtained from the simulations, consistent with the experimental spectra. A good fit to the experimental spectrum was obtained, without considering the quadrupolar interaction, since the size of this interaction is small in comparison to the dipolar interaction even at the low field strengths used here (4.7 T). This study demonstrates that the ^6Li MAS NMR spinning sideband manifolds are very sensitive to the arrangements of the first cation coordination sphere of Mn ions around the Li cations, providing a method for obtaining local structural information from these classes of materials.

Introduction

Lithium manganese(IV) oxide, Li_2MnO_3, adopts the rock salt structure, and has been widely studied, in part due to the recent effort to develop new lithium manganates for use as cathode materials in lithium rechargeable batteries.[1,2] Various space group symmetries have been reported for Li_2MnO_3,[1,3−5] which may be related to the apparent dependence of the cation distributions over the different octahedral sites in the ordered rock salt structure, the concentrations of cation vacancies, and the consequent variations in local site distortions on the preparation conditions. Relatively recently, two separate studies of the crystal structure of Li_2MnO_3 have been carried out. The structure was refined in a monoclinic space group in both reports, one report using *C*2/*m* and the other *C*2/*c*.[1,4] Three different crystallographic sites for the Li cations are present in both structures. The formula of Li_2MnO_3 can be rewritten as $Li[Li_{1/3}Mn_{2/3}]O_2$, and is structurally related to the layered compounds $LiMO_2$ (M = Co, Ni, Mn, Cr, etc). The layered (monoclinic) form of $LiMnO_2$ has alternating layers occupied by cations and Mn cations.[6,7] In Li_2MnO_3, however, one-third of the manganese in the manganese planes is replaced by Li.

Li_2MnO_3 has been studied by ^6Li and ^7Li MAS NMR spectroscopy.[8−10] Resonances from all three crystallographic sites were resolved, which could be assigned on the basis of their relative intensities and by considering the local arrangements of manganese about the lithium ions. In our previous lithium MAS NMR work on these and similar systems, we have used the lithium hyperfine shift as a method for investigating local structure.[10−13] The purpose of the research reported in this paper is to explore the information that can be obtained from the spinning sidebands that are typically seen in the spectra of these paramagnetic materials. Li_2MnO_3 represents an important model compound because of the structural similarities between this material and the $LiMO_2$ cathode materials used in lithium rechargeable batteries. Furthermore, the relatively recently synthesized layered materials $Li[Cr_xLi_yMn_{1-x-y}]O_2$ and $Li[Co_xMn_{1-x}]O_2$ are reported to contain regions or domains with cation ordering schemes that are similar to those found in Li_2MnO_3. These cathode materials have high reversible capacities and do not transform into spinel structure during the cycles and as such have received considerable attention.[14−16] Li_2MnO_3 may also be acid-leached to produce lithium manganate cathode materials with high reversible capacities in lithium cells, which can be described by the formula $Li_{2-x}MnO_{3-(x/2)}$.[2,17]

The ordered spinel phase $LiZn_{0.5}Mn_{1.5}O_4$ contains two sites for the lithium cations, i.e., a tetrahedral site and an octahedral site.[13] The Li cations in the octahedral site of ordered $LiZn_{0.5}Mn_{1.5}O_4$ and the 2b site of Li_2MnO_3 both have six manganese cations in the first coordination environment connected to 6 manganese ions via 12 Li−O−Mn interactions with bond angles of approximately 90°. In our earlier work, we showed that the size of the lithium hyperfine shifts obtained from the lithium NMR spectra of these classes of materials could be readily rationalized by considering the number of manganese ions in the lithium coordination sphere and the Li−O−Mn bond angles. On the basis of this work, both compounds are predicted to have very similar hyperfine interactions and thus very similar lithium-6 or -7 shifts.[10,13] However, the geometric arrangements of the Mn ions about the Li cation and the site symmetries are different: the 2b site of Li_2MnO_3 has 2/*m* symmetry, while the 4a site of $LiZn_{0.5}Mn_{1.5}O_4$ is located on a 3-fold rotation axis. This should be reflected in their corresponding NMR spectra. The local coordination environment and the NMR shift corresponding to each site are listed in Table 1.

* To whom correspondence should be addressed.

10.1021/jp013224s CCC: $22.00 © 2002 American Chemical Society
Published on Web 03/19/2002

TABLE 1: Local Environment for the Lithium Cations in the Different Sites in Li_2MnO_3 and $LiZn_{0.5}Mn_{1.5}O_4$ and the Observed NMR Shifts Obtained by Different Research Groups

		Li−O−Mn bond angle (deg)	no. of bonds	Li NMR shift (ppm) ref 8	ref 9	our data
	site					
Li_2MnO_3	2b (4e)[a]	90	12	1817	1770	1460
	2c (4d)	90	8	922	875	755
		180	4			
	4h (8f)	90	8	905	850	734
		180	4			
$LiZn_{0.5}Mn_{1.5}O_4$	4a (tet)	122	12			684
	4a (oct)	90	12			2325

[a] The Wyckoff site label in the space group *C*2/*c* is given in parentheses.

In paramagnetic solids, both the isotropic part of the Fermi contact (or hyperfine) interaction and typically much smaller pseudocontact shift lead to a shift of the resonance from the typical chemical shift position expected for a diamagnetic solid. In addition, large spinning sideband (ssb) manifolds, which spread over a large spectral width, are observed due to the anisotropic dipolar coupling interaction between the electronic and nuclear moments. We shall refer to this interaction as the paramagnetic dipolar interaction. This interaction contains structural information regarding the arrangement of the paramagnets surrounding the nucleus of interest. As a result, a number of studies have been carried out to establish a theoretical background and to simulate the NMR spectra of paramagnetic solids.[18−23,24]

The Hamiltonian describing the paramagnetic dipolar interaction resembles the chemical shielding interaction, in that it scales linearly with the field.[19] Other sources of intensity in the ^{6}Li and ^{7}Li ssb manifolds include anisotropic interactions such as the dipolar interaction between two nuclei (which unlike the paramagnetic dipolar interaction is independent of the field strength), the chemical shielding anisotropy, the anisotropic part of the Fermi contact interaction, and the quadrupolar interaction. For ^{6}Li, these interactions are likely to be smaller than the paramagnetic interaction, but this assumption will be discussed in more detail below.

The ^{6}Li NMR spectra of Li_2MnO_3 and $LiZn_{0.5}Mn_{1.5}O_4$, which contain Li environments with two kinds of axial symmetry (oblate and prolate types), are presented in this paper. The spectral width and the intensity distribution of the ssbs are calculated using the known crystal structures. The structural refinement carried out in the space group $C2/m$[1] was used to analyze the spectra of Li_2MnO_3. Calculations were also performed by using the second refinement performed in space group $C2/c$,[4] but the results were very similar. The discrepancy between the experimental and simulated spectra is discussed.

Experimental Section

Sample Preparation. Li_2MnO_3 was prepared from Li_2CO_3 and Mn_2O_3 by solid-state methods. Stoichiometric amounts of the starting materials were ground together, formed into pellets, and heated at 650 °C for 12 h followed by 850 °C for 24 h in air. The sample was then slowly cooled to room temperature in the furnace. A sample of $LiZn_{0.5}Mn_{1.5}O_4$, in which the cations are ordered on both the octahedral and tetrahedral sites, was synthesized in air by conventional solid-state reactions, following the approach outlined in our earlier publication.[13] A pelletized mixture of Li_2CO_3, $MnCO_3$, and ZnO was heated at 700 °C for 48 h with intermittent grinding and was slowly cooled to room temperature at a controlled cooling rate of 1 °C/min. ^{6}Li-enriched Li_2CO_3 (Isotec; >95% ^{6}Li) was used for the ^{6}Li enrichment.

Solid-State NMR Spectroscopy. ^{6}Li MAS NMR experiments were performed at 29.47 MHz on a CMX-200 spectrometer (field strength 4.68 T) with a Chemagnetics probe equipped with a 4 mm (o.d.) rotor for MAS. A pulse width of 2.9 μs with a pulse delay of 0.5 s was used. A 1 M solution of LiCl was used as a secondary reference at 0 ppm. The spectrometer dead time results in a loss of the first few points of the FID signal, resulting in a distorted spectrum. To eliminate this, a spin−echo sequence (90°−τ−180°−τ−acq) was used, with a value of τ of 1 rotor period. Spinning speeds of 8.7−8.8 kHz were used to minimize the overlap between the ssbs of the different resonances. All experiments were carried out at 50 °C using a Chemagnetics VT stack to control the temperature. The temperature was not calibrated at the spinning speed chosen in these experiments, but the error is less than 18 °C on the basis of the temperature calibration plot previously performed for the same probe,[11] but at a faster spinning speed.

Methodology

The through-space dipolar coupling between the nuclear and electronic magnetic moments is similar to the dipolar interaction between nuclear spins. However, when the dipolar interaction involves a second set of coupled $I = 1/2$ nuclear spins, coupling to both the $|+1/2\rangle$ and $|-1/2\rangle$ eigenstates will occur, resulting in the classic Pake doublet pattern for a powder. In contrast, when the second set of coupled spins are electrons (or paramagnetic ions), the nuclear spins can only couple to the time-averaged magnetic moment, since the electronic relaxation time T_{1e} is typically extremely fast, on the NMR time scale. The line shape in this case resembles that of the chemical shift anisotropy. The Hamiltonian for this interaction can be represented by[19,25,26]

$$H_{en} = \frac{\mu_0}{4\pi}\bar{\mu}_e \cdot \tilde{D}_{en} \cdot \mu_N \tag{1}$$

where μ_0 denotes the permeability, $\bar{\mu}_e$ the time (or thermally) averaged magnetic moment of the electrons, $\tilde{D}_{en}$ the dipolar coupling tensor between the unpaired electron(s) and the nucleus, and μ_N the magnetic moment of the nucleus. The dipolar coupling tensor, $\tilde{D}_{en}$, is defined by its matrix elements as follows:[27,28]

$$D_{ij} = \frac{1}{r^3}(\delta_{ij} - 3e_i e_j) \tag{2}$$

where r is the distance between the nucleus and the unpaired electron, δ_{ij} is the Kronecker delta ($\delta_{ij} = 1$ for $i = j$ and 0 for $i \neq j$), and e_i and e_j are the x, y, and z components of a unit vector pointing from the nuclear spin to the electron spin in a chosen coordinate system. Assuming spin-only paramagnetism, the thermally averaged mean magnetic moment, $\bar{\mu}_e$, is defined by[29]

$$\bar{\mu}_e = \frac{{\mu_B}^2 S(S+1)}{3k_B T}\tilde{g} \cdot \tilde{g} \cdot B_0 \tag{3}$$

where μ_B is the Bohr magneton, S the electron spin quantum number, k_B Boltzmann's constant, $\tilde{g}$ the electron g-tensor, and B_0 the magnetic field strength.

When ions with a $3d^3$ electronic configuration are placed in an octahedral field, the ground state is an orbital singlet ($^4A_{2g}$) and all the excited states lie higher in energy by an amount that is much larger than the spin−orbit coupling.[30] Thus, g is essentially isotropic with a value equal or very close to that of the free electron case. Mixing of the excited states into the ground state can, however, occur. In such a case, the g value departs from the free-spin value, but the deviation in the case of Mn^{4+} is so small that g can be approximated to the free-spin value.[31,32] Li_2MnO_3 has been studied by EPR and magnetic susceptibility measurements.[33,34] A sharp, symmetric EPR signal was observed, with $g = 1.994$ (i.e., $g_{xx} \approx g_{yy} \approx g_{zz} \approx 1.994$).[34] Furthermore, a magnetic moment, extracted from the magnetic susceptibility data, of 3.91 μ_B was obtained, which is very close to the calculated spin-only value (3.87).[33] Thus, the use of the spin-only formula, and a value for g of 2 in eq 3 appears to be a reasonable assumption for both Mn^{4+} compounds. A spin angular momentum of $S = 3/2$ is used in eq 3 to calculate $\bar{\mu}_e$.

The geometric part of the dipolar coupling tensor in eq 1 is represented in spherical polar coordinates as[19]

$$\tilde{D}_{en} = \begin{bmatrix} d_{xx} & d_{xy} & d_{xz} \\ d_{yx} & d_{yy} & d_{yz} \\ d_{zx} & d_{zy} & d_{zz} \end{bmatrix} \tag{4}$$

$$d_{xx} = (1 - 3\sin^2\theta\cos^2\phi)/r^3$$

$$d_{xy} = (-3\sin^2\theta\cos\phi\sin\phi)/r^3$$

$$d_{xz} = (-3\sin\theta\cos\theta\cos\phi)/r^3$$

$$d_{yx} = (-3\sin^2\theta\cos\phi\sin\phi)/r^3$$

$$d_{yy} = (1 - 3\sin^2\theta\sin^2\phi)/r^3$$

$$d_{yz} = (-3\sin\theta\cos\theta\sin\phi)/r^3$$

$$d_{zx} = (-3\sin\theta\cos\theta\cos\phi)/r^3$$

$$d_{zy} = (-3\sin\theta\cos\theta\sin\phi)/r^3$$

$$d_{zz} = (1 - 3\cos^2\theta)/r^3$$

where θ and ϕ are the polar and azimuthal angles that define the angle that the dipolar vector makes with respect to a Cartesian axis system defined within the crystallographic frame and r is the distance between the nucleus and the paramagnetic ion. The systems under investigation in this paper are multispin systems. Since it is reasonable, as a first approximation, to assume that the electron spins function independently as local fields, the total dipolar coupling tensor can be obtained by performing a sum over all the spins out to infinity. To obtain the total interaction, all the tensors must be expressed in a common axis system. The crystallographic frame can be conveniently chosen as the axis system for orthorhombic, tetragonal, and cubic systems such that the x, y, and z axes are parallel to the crystallographic unit cell axes a, b, and c, respectively. For Li_2MnO_3, where the crystal symmetry is monoclinic, the x and y axes are chosen parallel to the a and b axes of the unit cell, respectively, and the z axis is taken as perpendicular to the x and y axes. The total Hamiltonian for the dipolar coupling, H_{en}, is then the sum of the individual coupling tensors for coupling to each individual paramagnetic ion, and the summation is performed numerically by including the Mn cations in successive coordination spheres:

$$H_{en} = \frac{\mu_0}{4\pi}\frac{\mu_B^2 S(S+1)}{3k_B T} g^2 B_0 \gamma_I \left(\sum_i \tilde{D}_{en,i}\right) I \tag{5}$$

where γ_I is the magnetogyric ratio of the nuclear spins and I is the nuclear spin quantum number. The transformation of the traceless dipolar coupling tensor into its own principal axis system (performed by diagonalization of the final coupling matrix) gives the eigenvalues for the shift anisotropy, δ_{zz}, δ_{xx}, and δ_{yy}. The convention $|\delta_{zz} - \delta_{iso}| \geq |\delta_{xx} - \delta_{iso}| \geq |\delta_{yy} - \delta_{iso}|$ is used to define the principal components of the tensor.[19] The shift anisotropy, $\Delta\delta$, and the asymmetry, η, are obtained from the eigenvalues as follows:

$$\Delta\delta = \frac{\delta_{xx} + \delta_{yy}}{2} - \delta_{zz} \tag{6}$$

$$\eta = \frac{\delta_{xx} - \delta_{yy}}{\delta_{iso} - \delta_{zz}} \tag{7}$$

where the sign and the size of $\Delta\delta$ depend on the site symmetry and the magnitude of the dipolar interaction, respectively, and η takes value from 0 to 1, representing by how much the spectral pattern deviates from axial symmetry. For example, in the case of axial symmetry (i.e., $\eta = 0$), an oblate-type arrangement is represented by a negative value of $\Delta\delta$ and a prolate arrangement by a positive $\Delta\delta$ value. These parameters were used to simulate the spectra by using a program written by Kwang Hun Lim within the GAMMA platform.[35,36]

Results and Discussion

^{6}Li NMR Spectra of Li_2MnO_3 and $LiZn_{0.5}Mn_{1.5}O_4$. The ^{6}Li NMR spectra of Li_2MnO_3 and $LiZn_{0.5}Mn_{1.5}O_4$ are shown in Figure 1. Three resonances are observed at 734, 755, and 1461 ppm for Li_2MnO_3, which have been assigned to the 4h, 2c, and 2b sites, respectively.[8] The similar local environments of the 4h and 2c sites result in similar hyperfine shifts, causing an overlap of the resonances. Both 4h and 2c sites show large ssb manifolds spanning ~3600 ppm. The ssbs arising from the 2b site are larger and extend over 4000 ppm. The ssb envelopes due to the 2b site and those from 4h and 2c sites are not symmetric about the isotropic resonance, both arising from environments with close to axial symmetry, but with opposite signs for the anisotropy parameter, $\Delta\delta$. Two resonances are seen at 684 and 2325 ppm in the spectrum of $LiZn_{0.5}Mn_{1.5}O_4$, due to Li in the tetrahedral and the octahedral sites, respectively.[13] The resonance due to Li in the tetrahedral site has a smaller line width, and the ssb manifold of this site (covering ~2600 ppm) is close to being symmetric about the isotropic resonance. In contrast, Li in the octahedral site gives rise to a resonance with what appears to be a close to axially symmetric powder pattern extending over 5000 ppm.

The different hyperfine shifts for Li in the octahedral site of $LiZn_{0.5}Mn_{1.5}O_4$ and 2b site of Li_2MnO_3 (2350 and 1460 ppm, respectively) are surprising, given the very similar Li−O−Mn connectivities. These differences must be related to the extent of Li−O and O−Mn orbital overlap. A careful examination of the Li−O and O−Mn bond lengths and Li−O−Mn bond angles does not, however, reveal any significant differences between the two compounds. The local coordination of the *oxygen* atoms

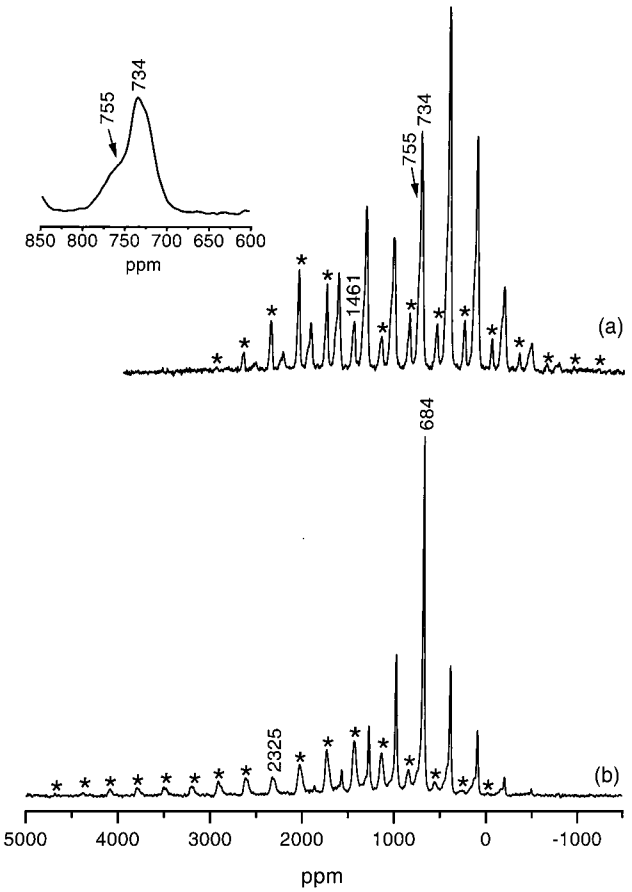

Figure 1. ^{6}Li MAS NMR spectra of (a) Li_2MnO_3 and (b) $LiZn_{0.5}Mn_{1.5}O_4$ acquired at a controlled temperature of 50 °C with spinning speeds of 8.7−8.8 kHz. Isotropic resonances are marked on the spectra; all other peaks are spinning sidebands. The asterisks denote the spinning sidebands of the resonances at 1461 and 2325 ppm. An expanded region of the spectrum of Li_2MnO_3 is shown as an inset in (a).

in these compounds is significantly different. The oxygen atom in the spinel is coordinated to three manganese/lithium ions in the octahedral site, and one lithium/zinc ion in the tetrahedral site. In contrast, the oxygen atoms in Li_2MnO_3 are octahedrally coordinated to six Li/Mn cations. Thus, it appears reasonable to suggest that the oxygen atom in the lower coordination environment will be more covalently bound to the nearby cations, resulting in stronger orbital overlap, and thus a noticeably larger hyperfine shift.

Calculation of the Paramagnetic Dipolar Coupling. It is noteworthy that the ssb patterns due to Li in the octahedral site of $LiZn_{0.5}Mn_{1.5}O_4$ and the 2b site of Li_2MnO_3 are characteristic of close-to-axial symmetry, but with an opposite sign of $\Delta\delta$. Li in the octahedral site of $LiZn_{0.5}Mn_{1.5}O_4$ and that in the 2b site of Li_2MnO_3 are both coordinated to six Mn cations in the first coordination sphere, but their local environments are very different. The arrangement of the Mn cations in the first coordination sphere of the 2b site of Li_2MnO_3 is an oblate-type arrangement, where the six manganese cations surrounding Li are coplanar and are arranged so as to form a hexagon (Figure 2a). In contrast, the Mn cations surrounding the Li cation in the octahedral site of $LiZn_{0.5}Mn_{1.5}O_4$ are distributed above and below an (imaginary) plane, so as to form a prolate-type arrangement (Figure 2b). The local coordination environment of the 4h site of Li_2MnO_3 is also shown in Figure 2c for comparison; the first coordination sphere contains four Mn ions connected through 90° Li−O−Mn bonds and resembles, to a first approximation, the prolate-type arrangement of $LiZn_{0.5}Mn_{1.5}O_4$, but with two of the Mn cations replaced by Li. The coordination environment of the 2c site of Li_2MnO_3 is very similar to that of the 4h site.

TABLE 2: Calculated Dipolar Interaction between the Nuclear and Electronic Moments for ^{6}Li Sites in Li_2MnO_3 and $LiZn_{0.5}Mn_{1.5}O_4$ Performed by Including Successive Coordination Spheres up to 10 Å

	2b, Li_2MnO_3		4a (Oh), $LiZn_{0.5}Mn_{1.5}O_4$	
	$\Delta\delta$ (ppm)	η	$\Delta\delta$ (ppm)	η
$6Mn_{(first)}$	−3544 (−3580)[a]	0.01	3373	0.00
$6Mn_{(first)} + 4Mn_{(second)}$	−2826 (−2866)	0.04	3133	0.00
$6Mn_{(first)} + 4Mn_{(second)} + 10Mn_{(third)}$	−3268 (−3012)	0.03	3134	0.00
up to 10 Å	−3000 (−2994)	0.03	3009	0.00

[a] The values calculated using the crystal structure refined in space group *C*2/*c* from ref 4 are given in parentheses.

The dipolar interaction between the paramagnetic and nuclear spins can be calculated by using the known crystallographic structure. In a point dipole approximation, the local field induced by other manganese cations is assumed to be negligible, and each manganese cation is approximated as a point dipole.[37,38] The manganese cations in each coordination sphere were successively included in the calculation, and the principal values were observed to converge at approximately 10 Å. The presence of the pseudo-6-fold rotation axis at the 2b site in the first coordination sphere of Li_2MnO_3 and the C_3 symmetry element at the Li cation in the octahedral site of $LiZn_{0.5}Mn_{1.5}O_4$ result in close-to-axial and axial symmetry, respectively. The calculated results are listed in Table 2. As expected, asymmetry values of 0 or close to 0 are obtained, and the anisotropy values for Li_2MnO_3 and $LiZn_{0.5}Mn_{1.5}O_4$ have opposite signs. The results should be compared with the values for $\Delta\delta$ and η of 1182 ppm and 0, respectively, for coupling to a single manganese ion 2.47 Å from the central lithium ion (2.47 Å representing the average Li−Mn interatomic distance in Li_2MnO_3). The arrangement of manganese ions in Li_2MnO_3 is such that the sum of the dipolar coupling tensors for each individual Li−Mn coupling partially cancels and results in an inversion in the sign of $\Delta\delta$. This can be readily rationalized: The principal value of the individual dipolar coupling tensor that describes the coupling to one of the six manganese ions in the first cation coordination sphere (δ_{zz}) points toward the individual manganese ion. To simplify the summation, δ_{xx} and δ_{yy} can be defined as being located in the plane of the six manganese ions and perpendicular to this plane, respectively. The total tensor for an axially symmetric local environment is easily calculated, since the principal value must by definition lie along the principal axis (i.e., perpendicular to the manganese plane in Li_2MnO_3). Thus, the total tensor for coupling to six manganese ions has principal values of $6\delta_{yy}$, $6(\delta_{xx} + \delta_{zz})/2$, and $6(\delta_{xx} + \delta_{zz})/2$, the principal axis $6\delta_{yy}$ now lying perpendicular to the manganese plane and differing in sign from the principal value for the dipolar coupling tensor for coupling to a single paramagnetic ion.

Assuming that the paramagnetic interaction is the dominant one in these systems, the spectra are simulated using the parameters listed in Table 2. The results are shown in Figures 3 and 4, where the isotropic resonances for both environments are set at 0 ppm for convenience. It is noteworthy that the calculation of the dipolar interaction using the crystal structure yields spectra with sidebands with anisotropies of the correct magnitude and sign. However, the agreement between the experimental and calculated spectra is only reasonable, and it is clear that total agreement cannot be obtained by considering

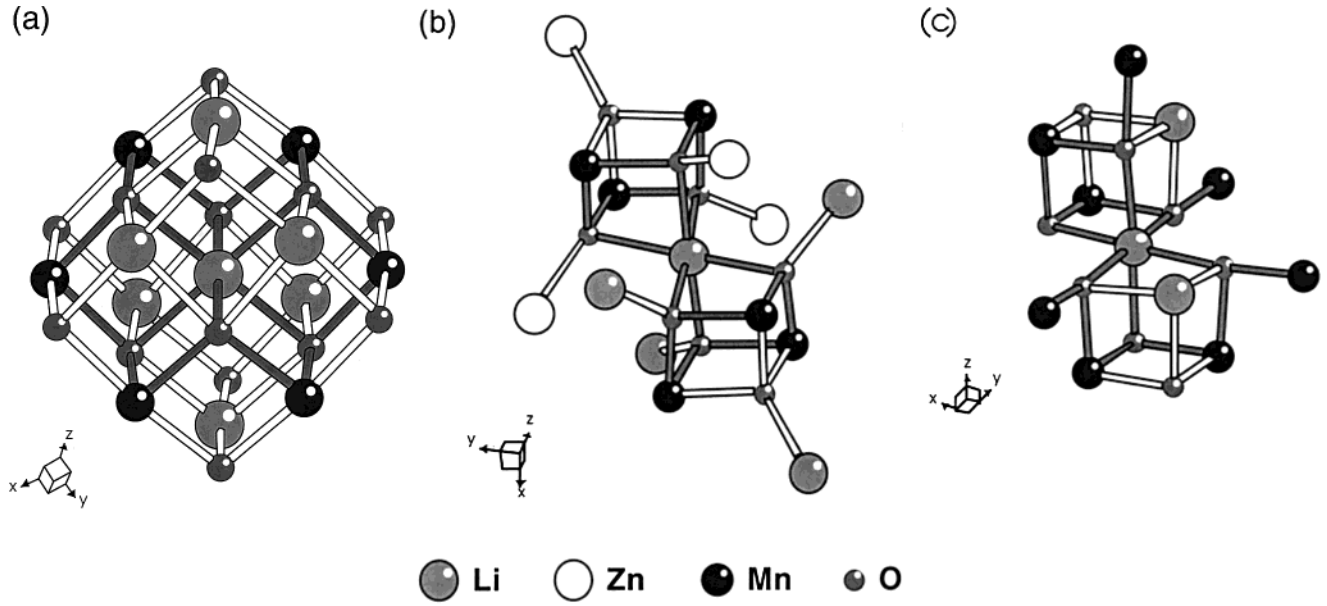

Figure 2. Local coordination environment of the lithium cations (a) in the 2b site of Li_2MnO_3, (b) in the octahedral sites of $LiZn_{0.5}Mn_{1.5}O_4$, and (c) in the 4h site of Li_2MnO_3. The Li−O−Mn connectivities around the central lithium cations are shaded.

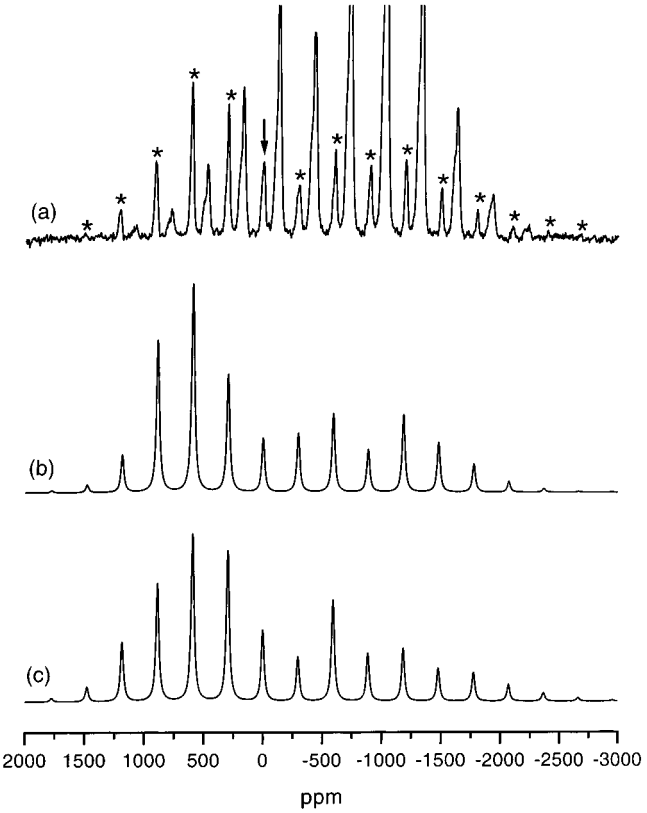

Figure 3. Experimental and simulated ^{6}Li MAS NMR spectra of Li_2MnO_3: (a) experimental spectrum, (b) calculated spectrum using the values of the electron−nuclear dipolar interaction reported in Table 2, and (c) calculated spectrum including both the dipolar and quadrupolar interactions (QCC = 20 kHz). The Euler angles (α, β, γ) used in this calculation are (0°, 0°, 0°). The isotropic resonance due to Li in the 2b site is marked with an arrow, and the ssbs from that site are indicated by asterisks.

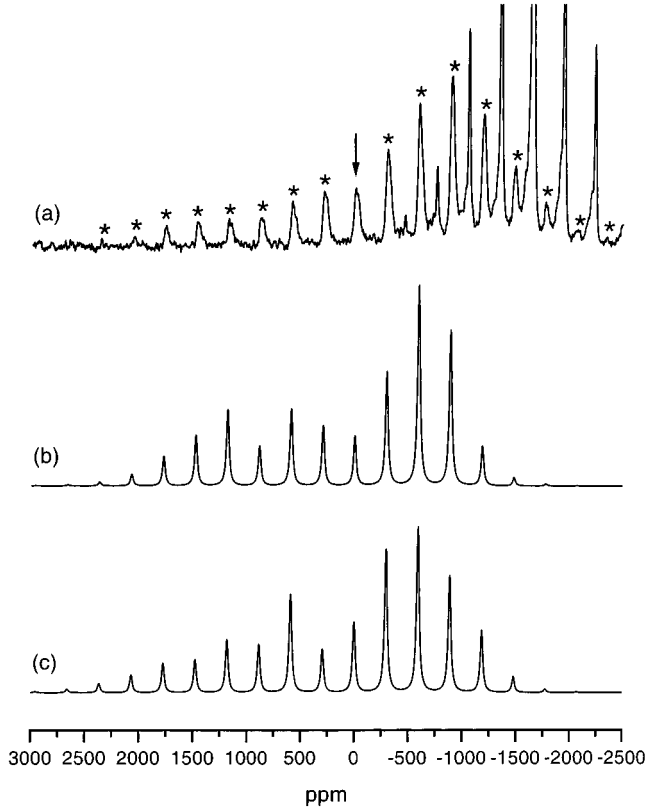

Figure 4. Experimental and simulated ^{6}Li MAS NMR spectra of $LiZn_{0.5}Mn_{1.5}O_4$: (a) experimental spectrum (the isotropic resonance due to the lithium cation in the octahedral site is marked with arrow; asterisks denote the ssb pattern from the octahedral site), (b) calculated spectrum using the values of the electron−nuclear dipolar interaction reported in Table 2, and (c) calculated spectrum including both the dipolar and quadrupolar interactions (QCC = 20 kHz). α, β, and γ are all set at 0°.

the paramagnetic interaction only. Attempts to extract experimental values of $\Delta\delta$ and η from the experimental spectra (by using, for example, a Hertzfeld−Berger (HB) analysis[39]) indicate that the anisotropic part of these resonances cannot be described by a single second-rank tensor. Rather, the experimentally observed sideband manifolds must be due to a number of different anisotropic interactions, so that the overall spectrum comprises a sum of more than one second-rank tensor. Importantly, however, similar values of $\Delta\delta$ are obtained by the calculation of the paramagnetic dipolar coupling, experimentally indicating that the paramagnetic dipolar coupling must be the dominant interaction.

The quadrupolar coupling was included in the simulation in an attempt to improve the fit. The paramagnetic coupling tensor and quadrupolar coupling tensor were initially assumed to be coincident, and then the orientation between two tensors (Euler angles) was systematically varied. However, no significant improvement in the spectral fit was obtained particularly for the $LiZn_{0.5}Mn_{1.5}O_4$ spectrum, and the spectra became more symmetric when a large quadrupolar coupling constant (QCC) was employed (QCC > 20 kHz), which is not consistent with the experimental spectra. These simulations suggest that the QCCs for the ^{6}Li sites are small, and thus, the quadrupolar interaction does not contribute to the intensity of ssbs significantly. The small ^{6}Li QCCs are consistent with the small ^{7}Li QCCs determined for various related materials. For example, ^{7}Li QCCs of 40−110 kHz were determined for a variety of ionic compounds (e.g., LiOH, $LiNO_3$, Li_2ZrO_3) by Hon et al.,[40] and QCCs of 30−130 and 3−40 kHz for $Li_xV_2O_5$ and $LiCoO_2$, respectively, were more recently determined by Hirschinger et al.[41,42] The ^{6}Li isotope will have a significantly smaller QCC, since the quadrupolar moment of ^{6}Li is much smaller than that of ^{7}Li ($Q(^7Li)/Q(^6Li) \approx 56$) and is thus negligible in comparison to the dipolar interaction.

There are several possible additional anisotropic interactions that could contribute to the intensities of the sidebands. In the Li NMR study of $LiCoO_2$, an improved fit was achieved by including the dipolar interaction between ^{6}Li/^{7}Li spins in the simulations of the ssb intensities.[42] However, the dipolar coupling involving unpaired electrons will be more than 4000 times larger than that to the ^{6}Li nuclei ($\gamma_e/\gamma_{6Li} = -4472$). Furthermore, no significant difference in the sideband patterns is seen for ^{6}Li-enriched and nonenriched samples, again suggesting that the contribution due to the dipolar interaction between the Li nuclei in Li_2MnO_3 and $LiZn_{0.5}Mn_{1.5}O_4$ is small. The effect of the bulk magnetic susceptibility (BMS) should also be considered. There are two sources for the BMS: A magnetic field is induced in each particle in a powder, when it is placed in the magnetic field. The local field induced in one particle will be felt by other particles, resulting in inhomogeneous broadening.[43] The induced field (the demagnetizing field) is also dependent on the particle shape and the orientation of the particle in the field, producing another source of broadening for nonspherical particules.[44−46] The inhomogeneous broadening caused by the BMS effect will be removed by fast MAS, but for paramagnetic systems, where the effect can be quite large, this effect can result in large sideband intensities due to incomplete averaging of this interaction. Various models have been proposed to allow the size of this interaction to be estimated and to calculate the change in the ssbs in the NMR spectra of paramagnetic compounds due to the BMS effect.[24,43,47] In our earlier ^{119}Sn study of lanthanum stannates, this interaction was found to be a major source of sideband intensity, making it difficult to extract accurate parameters for the dipolar coupling tensor from the sideband manifolds.[24] In this system, the BMS effect was reduced by susceptibility matching (i.e., by making suspensions of the paramagnetic powders in a liquid with a susceptibility similar to that of the solid). The calculated dipolar coupling tensors are larger than those found in these stannate materials, suggesting that the effect will be less severe. For example, for $Nd_2Sn_2O_7$ and $Pr_2Sn_2O_7$, values for $\Delta\delta$ of only approximately 300 ppm were observed, while the effective magnetic moments of these ions (3.5 μ_B) are only slightly smaller than that of Mn^{4+}. Nonetheless, the earlier studies do indicate that some caution must be exercised in extracting dipolar coupling tensors from systems with small dipolar couplings, but large magnetic susceptibilities. Since our aim was to develop a simple method to obtain structural information from the spectra, a more detailed analysis of the BMS is beyond the scope of this paper. It should be noted, however, that the fit of the spectra is good, using our simple model, considering the number of approximations that were made in calculating the spectra.

Conclusions

The spinning sidebands in the NMR spectra of paramagnetic materials contain information concerning the distributions of the paramagnets surrounding a nuclear spin. In this work, we have shown that the contribution to the ssb intensities due to the dipolar coupling between paramagnetic ions and nuclear spins in lithium manganates can be readily calculated from structural information. The calculations were performed by assuming that the dipolar interaction between the nuclear and the electronic magnetic moments was the dominant interaction, that each manganese cation may be approximated as a point dipole, and that the effects of the electron delocalization may be ignored; the theoretical calculations agree reasonably well with the experimental data. Depending on the arrangement of the paramagnetic manganese(IV) cations, two types of sideband patterns due to spins in axially symmetric environments were observed both experimentally and in the calculations (i.e., oblate and prolate types for the 2b site in Li_2MnO_3 and the octahedral site in $LiZn_{0.5}Mn_{1.5}O_4$, respectively). The ^{6}Li quadrupolar coupling constant appears to be very small and cannot be determined accurately even for the spectra acquired at the relatively low field strength used here (4.68 T). The slight discrepancies between the calculated and experimental sideband intensities are attributed primarily to bulk magnetic susceptibility broadening. The local coordination environments of the 4h and 2c sites of Li_2MnO_3 contain manganese ions in a pseudo-prolate-type arrangement, and are thus similar to the octahedral site in $LiZn_{0.5}Mn_{1.5}O_4$. However, the number of Mn cations in the nearest coordination sphere is reduced to four, in comparison to six in $LiZn_{0.5}Mn_{1.5}O_4$. Thus, smaller values of the anisotropy are expected for these sites, consistent with the experimental spectrum.

The relative contributions of the electron−nuclear dipolar coupling, the quadrupolar interaction, and the nuclear−nuclear dipolar interaction can be tuned by varying the magnetic field strength and varying the ^{6}Li enrichment level. Analysis of the electron−nuclear dipolar interaction, in the presence of a large QCC, should become more straightforward at higher fields. By choosing the appropriate (high) field, it may be possible to ignore this interaction, even when ^{7}Li MAS NMR spectra are analyzed. Our recent experiments with very fast MAS, utilizing spinning frequencies of over 45 kHz, suggest that this approach is feasible.

The importance of the oxygen coordination number in determining the size of the hyperfine shift was suggested in this work, smaller coordination numbers apparently resulting in larger shifts. Finally, this work shows that the analysis of the lithium NMR spinning sidebands provides a method for obtaining information that complements the structural data that can be extracted from the hyperfine interaction. The approach should prove useful, for example, to help determine whether lithium cations in disordered or cycled $LiMO_2$-related cathode materials reside between the transition metal (M) layers, or in the M layers, information that is difficult to obtain from other structural techniques.

Acknowledgment. Financial support from the National Science Foundation via Grant DMR 9901308 and a POWRE award to C.P.G. (Grant DMR-0074858) is gratefully acknowledged.

References and Notes

(1) Strobel, P.; Lambert-Andron, B. *J. Solid State Chem.* **1988**, *75*, 90.

(2) Roussouw, M. H.; Thackeray, M. M. *Mater. Res. Bull.* **1991**, *26*, 463.

(3) Lang, G. *Z. Anorg. Allg. Chem.* **1966**, *348*, 246.

(4) Riou, A.; Lecerf, A.; Gerault, Y.; Cudennec, Y. *Mater. Res. Bull.* **1992**, *27*, 269.

(5) Meyer, V. G.; Hoppe, R. *Z. Anorg. Allg. Chem.* **1976**, *424*, 257.

(6) Armstrong, A. R.; Bruce, P. G. *Nature* **1996**, *381*, 499.

(7) Tabuchi, M.; Ado, K.; Kobayashi, H.; Kageyama, H.; Masquelier, C.; Kondo, A.; Kanno, R. *J. Electrochem. Soc.* **1998**, *145*, L49.

(8) Morgan, K. R.; Collier, S.; Burns, G.; Ooi, K. *J. Chem. Soc., Chem. Commun.* **1994**, 1719.

(9) Mustarelli, P.; Massarotti, V.; Bini, M.; Capsoni, D. *Phys. Rev. B* **1997**, *55*, 12018.

(10) Lee, Y. J.; Wang, F.; Grey, C. P. *J. Am. Chem. Soc.* **1998**, *120*, 12601.

(11) Lee, Y. J.; Grey, C. P. *Chem. Mater.* **2000**, *12*, 3871.

(12) Lee, Y. J.; Eng, C.; Grey, C. P. *J. Electrochem. Soc.* **2001**, *148*, A249.

(13) Lee, Y. J.; Park, S.-H.; Eng, C.; Parise, J. B.; Grey, C. P. *Chem. Mater.* **2002**, *14*, 194.

(14) Armstrong, A. R.; Gitzendanner, R.; Robertson, A. D.; Bruce, P. G. *Chem. Commun.* **1998**, 1833.

(15) Ammundsen, B.; Desilvestro, J.; Groutso, T.; Hassell, D.; Metson, J. B.; Regan, E.; Steiner, R.; Pickering, P. J. *J. Electrochem. Soc.* **2000**, *147*, 4078.

(16) Paulsen, J. M.; Thomas, C. L.; Dahn, J. R. *J. Electrochem. Soc.* **1999**, *146*, 3560.

(17) Johnson, C. S.; Korte, S. D.; Vaughey, J. T.; Thackeray, M. M.; Bofinger, T. E.; Shao-Horn, Y.; Hackney, S. A. *J. Power Sources* **1999**, *81*−*82*, 491.

(18) Woehler, S. E.; Wittebort, R. J.; Oh, S. M.; Hendrickson, D. N.; Inniss, D.; Strouse, C. E. *J. Am. Chem. Soc.* **1986**, *108*, 2938.

(19) Nayeem, A.; Yesinowski, J. P. *J. Chem. Phys.* **1988**, *89*, 4600.

(20) Brough, A. R.; Grey, C. P.; Dobson, C. M. *J. Chem. Soc., Chem. Commun.* **1992**, 742.

(21) Brough, A. R.; Grey, C. P.; Dobson, C. M. *J. Am. Chem. Soc.* **1993**, *115*, 7318.

(22) Lin, T.-H.; DiNatale, J. A.; Vold, R. R. *J. Am. Chem. Soc.* **1994**, *116*, 2133.

(23) Lee, H.; Polenova, T.; Beer, R. H.; McDermott, A. E. *J. Am. Chem. Soc.* **1999**, *121*, 6884.

(24) Grey, C. P.; Dobson, C. M.; Cheetham, A. K. *J. Magn. Reson.* **1992**, *98*, 414.

(25) Cheetham, A. K.; Dobson, C. M.; Grey, C. P.; Jakeman, R. J. B. *Nature* **1987**, *328*, 706.

(26) Grey, C. P.; Dobson, C. M.; Cheetham, A. K.; Jakeman, R. J. B. *J. Am. Chem. Soc.* **1989**, *111*, 505.

(27) Mehring, M. *Principles of High-Resolution NMR in Solids*; Springer-Verlag: New York, 1983.

(28) Haeberlen, U. *Advances in Magnetic Resonance*; Academic Press: New York, 1976; Suppl. 1.

(29) Bloembergen, N. *Physica* **1950**, *16*, 95.

(30) Abragam, A.; Bleaney, B. *Electron Paramagnetic Resonance of Transition Ions*; Dover Publications: New York, 1986.

(31) Goodenough, J. B. *Magnetism and the Chemical Bonding*; John Wiley & Sons: New York, 1963; Chapter 1.

(32) Hatfield, W. E. *Solid State Chemistry Techniques*; Oxford University Press: Oxford, U.K., 1987.

(33) Massarotti, V.; Capsoni, D.; Bini, M.; Chiodelli, G.; Azzoni, C. B.; Mozzati, M. C.; Paleari, A. *J. Solid State Chem.* **1997**, *131*, 94.

(34) Massarotti, V.; Capsoni, D.; Bini, M.; Azzoni, C. B.; Paleari, A. *J. Solid State Chem.* **1997**, *128*, 80.

(35) Smith, S. A.; Levante, T. O.; Meier, B. H.; Ernst, R. R. *J. Magn. Reson.* **1994**, *106A*, 75.

(36) Lim, K. H. Ph.D. Dissertation, State University of New York at Stony Brook, Stony Brook, NY, 2000.

(37) McConnell, H. M. *J. Chem. Phys.* **1957**, *27*.

(38) Pople, J. A. *J. Chem. Phys.* **1956**, *24*, 1111.

(39) Herzfeld, J.; Berger, A. E. *J. Chem. Phys.* **1980**, *73*, 6021.

(40) Hon, J. F.; Bray, P. J. *Phys. Rev.* **1958**, *110*, 624.

(41) Hirschinger, J.; Mongrelet, T.; Marichal, C.; Granger, P.; Savariault, J.-M.; Déramond, E.; Galy, J. *J. Phys. Chem.* **1993**, *97*, 10301.

(42) Siegel, R.; Hirschinger, J.; Carlier, D.; Matar, S.; Ménétrier, M.; Delmas, C. *J. Phys. Chem. B* **2001**, *105*, 4166.

(43) Drain, L. E. *Proc. Phys. Soc.* **1962**, *80*, 1380.

(44) Dickinson, W. C. *Phys. Rev.* **1951**, *81*, 717.

(45) VanderHart, D. L.; Earl, W. L.; Garroway, A. N. *J. Magn. Reson.* **1981**, *44*, 361.

(46) Alla, A.; Lippmaa, E. *Chem. Phys. Lett.* **1982**, *87*, 30.

(47) Kubo, A.; Spaniol, T. P.; Terao, T. *J. Magn. Reson.* **1998**, *133*, 330.